

Andreev reflection in graphene nanoribbons

Diego Rainis,¹ Fabio Taddei,¹ Fabrizio Dolcini,¹ Marco Polini,¹ and Rosario Fazio^{2,1}

¹*NEST-CNR-INFM and Scuola Normale Superiore, I-56126 Pisa, Italy*

²*International School for Advanced Studies (SISSA), via Beirut 2-4, I-34014 Trieste, Italy*

(Dated: November 1, 2021)

We study Andreev reflection in graphene nanoribbon/superconductor hybrid junctions. By using a tight-binding approach and the scattering formalism we show that finite-size effects lead to notable differences with respect to the bulk graphene case. At subgap voltages, conservation of pseudoparity, a quantum number characterizing the ribbon states, yields either a suppression of Andreev reflection when the ribbon has an even number of sites in the transverse direction or perfect Andreev reflection when the ribbon has an odd number of sites. In the former case the suppression of Andreev reflection induces an insulating behavior even when the junction is biased; electron conduction can however be restored by applying a gate voltage.

PACS numbers: 74.45.+c, 73.23.-b, 72.10-d

I. INTRODUCTION

Graphene, a flat monolayer of Carbon atoms arranged in a two-dimensional (2D) honeycomb lattice, is a newly realized 2D electron system¹ which has attracted a great deal of interest because of the novel physics which it exhibits and because of its potential as a new material for electronic technology. One of the fascinating aspects of this system is that in most cases its potentialities for device applications are intimately related with fundamental aspects of quantum mechanics. Many of the transport properties of graphene which are at the heart of the design of new functional nanostructures originate from conservation laws of certain quantum numbers. For example, the fact that electrostatic barriers in graphene are perfectly transparent to electrons scattering with angles close to normal incidence (Klein-paradox) is explained² in terms of conservation of pseudospin (the sublattice degree-of-freedom necessary to describe graphene's non-Bravais honeycomb lattice¹).

Early investigations on transport properties of graphene have analyzed current and noise in the presence of normal leads. Recent studies^{3,4,5,6,7,8,9} have pointed out that novel interesting phenomena arise when graphene is interfaced to a superconductor (SC). In the seminal papers by Beenakker and coworkers³ it has been shown that the peculiar band structure of graphene gives rise to the appearance of specular Andreev reflection (AR)¹⁰, a novel type of AR that is absent in ordinary metal/SC interfaces. These studies paved the way to experimental investigations of the proximity effect^{11,12} and of supercurrent flow^{13,14} in graphene. On the theoretical side the results of Ref. 3 have been extended in a number of ways, *e.g.* to graphene bilayers⁴ and to the case of interfaces with *d*-wave SCs⁵, whereas further studies have focused on the subgap structure of SC-graphene-SC junctions⁶, on crossed AR⁷, and on magneto-transport⁸.

Most of the theoretical analysis carried out so far describe the graphene sheet as an infinite (or semi-infinite) 2D plane, and identify two energy scales relevant for transport, namely the superconducting gap Δ_0 and the

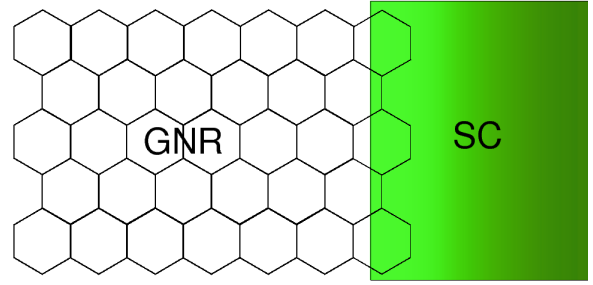


FIG. 1: (Color online) A hybrid junction between a zigzag graphene nanoribbon and a superconductor.

potential difference between the normal side and the superconducting side, which allows, for instance, to switch from the regime of ordinary AR to the one of specular AR. In graphene ribbons¹⁵, however, the finite size of the sample yields an additional energy scale δ , characterizing the mean energy spacing between the ribbon bands. Since the typical ribbon size varies from 10 nm up to 1 μm ¹⁵, δ can range from 300 meV down to 3 meV, and it is thus larger than (or of the same order of) the typical superconducting gap $\Delta_0 \lesssim 1$ meV. As a consequence, δ is expected to play an important role in electron transport and AR in graphene.

In the present work we address this problem by analyzing electronic transport through a hybrid junction between a Graphene NanoRibbon (GNR)^{16,17,18} and a SC, as sketched in Fig. 1. We consider the case of a GNR with zigzag edges, which has been shown to represent fairly well the behavior of an arbitrarily shaped edge¹⁹.

Novel effects emerge due to the finite size of the GNR. We find that AR is strongly affected by the conservation of *pseudoparity*, a quantum number characterizing the GNR eigenstates, which depends on whether the number N_W of sites along the transverse direction is even or odd. In particular, while in GNRs with odd N_W the AR coefficient is unity for subgap voltages, in GNRs with an

even N_W AR is totally suppressed. In the latter case AR can be restored to a finite value by applying a gate voltage. Even-odd effects with the same physical origin have been also found in normal transport through graphene p-n junctions (valley-valve effect)^{20,21,22}.

The contents of the paper are briefly described as follows. In Sect. II we introduce the tight-binding Hamiltonian that we use to model the GNR and provide analytical expressions for the GNR eigenfunctions at arbitrary energy, briefly discussing how transport properties of the hybrid GNR/SC junction are calculated. In Sect. III we report and discuss our results. Finally, in Sect. IV we summarize our main conclusions.

II. MODEL HAMILTONIAN, GNR EIGENFUNCTIONS, AND TRANSPORT PROPERTIES

We model the hybrid GNR/SC system by means of a tight-binding approach. In order to interpret the results presented below, we start by describing the eigenstates in the “normal” side of the junction (the GNR side). The GNR Hamiltonian \mathcal{H} is a matrix with elements $\mathcal{H}_{ij} = -\gamma\delta_{\langle i,j \rangle} + U\delta_{ij}$, where $\gamma \simeq 2.8$ eV is the hopping energy between nearest-neighbor sites $\langle i, j \rangle$ on the honeycomb lattice, and U accounts for a constant electrostatic energy, which can be controlled by a gate voltage.

Denoting by \mathbf{a}_1 and \mathbf{a}_2 the honeycomb-lattice basis, each unit cell is labeled by a vector $\mathbf{r} = n_1\mathbf{a}_1 + n_2\mathbf{a}_2$, with n_1 and n_2 integers. The origin is located at the geometrical center of the GNR and N_W is the number of sites in the transverse direction $\hat{\mathbf{e}}_y$. A suitable shape of the cells turns out to depend on whether N_W is even or odd, as depicted in Fig. 2. It can be shown that the (unnormalized) eigenfunctions of a zigzag GNR at a cell $\mathbf{r} = (x, y)$ are given by²³

$$\Psi_{A(B),s}(x, y) = e^{ik_x x_{A(B)}(x)} \Phi_{A(B),s}(y) \quad (1)$$

where $x_{A(B)}(x)$ is the coordinate of the $A(B)$ site of the cell along the longitudinal direction $\hat{\mathbf{e}}_x$, $\Phi_{A(B),s}$ is the wavefunction along the transverse direction at $A(B)$, and $s = \uparrow, \downarrow$ is a spin label. Explicitly, $x_{A(B)} = x$ if N_W is even, whereas $x_{A(B)} = x \mp a\sqrt{3}/4$ if N_W is odd ($a \simeq 1.42$ Å is the Carbon-Carbon distance). Furthermore

$$\begin{pmatrix} \Phi_{A,s}(y) \\ \Phi_{B,s}(y) \end{pmatrix} = \begin{pmatrix} \sin[k_y(W/2 + y)] \\ \eta \sin[k_y(W/2 - y)] \end{pmatrix} \quad (2)$$

where $W \doteq 3a \text{int}[(N_W + 1)/2]$ approximately coincides with the width of the GNR, with $\text{int}[x]$ denoting the integer part of x . The eigenvalues related to (1) read

$$\varepsilon = U + \eta \gamma \Re e f(k_x a \sqrt{3}, 3k_y a) \quad (3)$$

where

$$f(\xi, \kappa) = e^{i\kappa N_W/2} [1 + 2e^{i\kappa/2} \cos(\xi/2)], \quad (4)$$

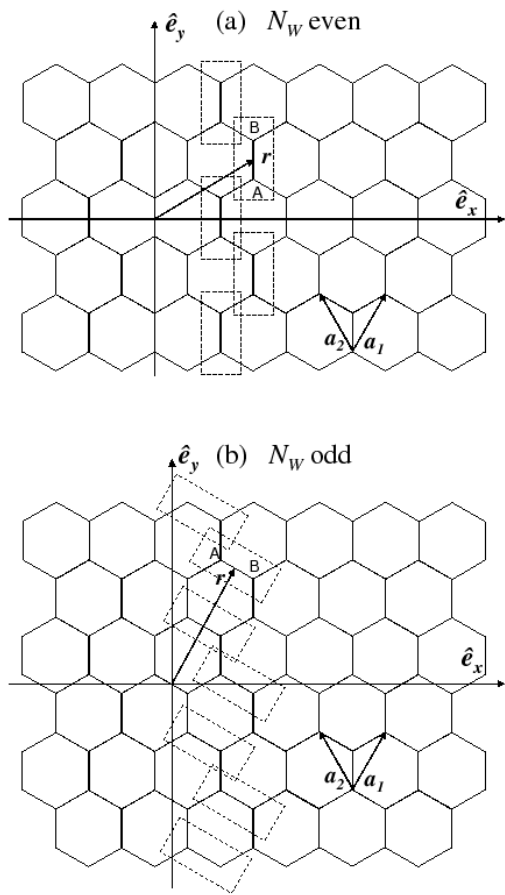


FIG. 2: Coordinates and elementary cells in GNRs with (a) an even number of sites in the transverse direction $\hat{\mathbf{e}}_y$ and (b) an odd number of sites in the $\hat{\mathbf{e}}_y$ direction.

and k_y is the solution of $\Im m f(k_x a \sqrt{3}, 3k_y a) = 0$ (see also Ref. 18). The quantity k_x (k_y) is the component of the momentum along $\hat{\mathbf{e}}_x$ ($\hat{\mathbf{e}}_y$). Importantly, beside the momentum, the eigenstates defined in Eqs. (1)-(2) exhibit an additional quantum number $\eta = \pm 1$, which determines whether the transverse cell wavefunction $(\Phi_A + \Phi_B)/2$ is even or odd with respect to the longitudinal axis of the GNR. One can therefore term η as *pseudoparity*. Note that, in contrast to what happens in bulk graphene, the states (1)-(2) are not eigenstates of the pseudospin-projection operator $\boldsymbol{\sigma} \cdot \hat{\mathbf{n}}$ for any unit vector $\hat{\mathbf{n}}$.

The eigenvalues ε as functions of k_x describe the band structure of the zigzag GNR, where two bands exhibit dispersionless zero modes and the other ones are somewhat reminiscent of the bulk-graphene Dirac cones¹, as illustrated in Fig. 3 for the case $U = 0$. Energies are measured with respect to the Fermi level, and solid (dashed) lines refer to particles (holes) bands, which are degenerate for this particular case. The value of the pseudoparity η , shown inside the circles, alternates from a particle band to the next one, and takes opposite values in particle and hole bands. Importantly, in the range

$k_x a \sqrt{3} \in [0, \pi]$, the pseudoparity of a GNR with even N_W is opposite to the one for the case with odd N_W .

The energy separation δ between the first band and the zero-mode energy (Dirac level) is given by $\delta \simeq 9\pi\gamma/(6N_W - 4)$ for even $N_W \gg 1$ or $\delta \simeq 3\pi\gamma/(2N_W - 2)$ for odd $N_W \gg 1$ ²⁴. A finite U shifts the energy of the Dirac level away from the Fermi level, as shown in Fig. 4, breaking particle-hole degeneracy.

The presence of the superconducting electrode is accounted for by the Bogoliubov-de Gennes Hamiltonian²⁵

$$\mathcal{H}_{\text{BdG}} = \begin{pmatrix} \mathcal{H} - \varepsilon_F & \Delta \\ \Delta^* & \varepsilon_F - \mathcal{H}^* \end{pmatrix}, \quad (5)$$

where \mathcal{H} is the particle Hamiltonian, and ε_F is the Fermi level of the GNR/SC junction at equilibrium. The SC (s -wave) order parameter, which couples particles and holes, is described by a matrix Δ with entries $\Delta_{ij} = \Delta_i \delta_{ij}$. Here Δ_i is taken to vary smoothly across the junction, between its maximum value Δ_0 in the bulk of the SC and zero in the bulk of the GNR²⁶.

Within the scattering approach²⁷ the zero-temperature differential conductance is given by²⁸

$$G(V) = \frac{4e^2}{h} [N(V) - R(V) + R_A(V)], \quad (6)$$

where V is the bias voltage applied across the junction. In Eq. (6) the prefactor 4 is due to spin and valley degeneracies, whereas $N(V)$, $R(V)$ and $R_A(V)$ are the number of transverse propagating modes (open channels) available at energy eV measured from the Fermi level ε_F , the normal reflection coefficient, and the AR coefficient, respectively. Below the gap ($eV < \Delta_0$) only AR processes can contribute to the conductance, since the unitarity of the scattering matrix implies that $N - R = R_A$ in this range.

III. RESULTS AND DISCUSSION

We present our numerical results focusing on the physically realistic regime $\delta \gg \Delta_0$. We first discuss the case where the Fermi level lies at the Dirac level ($U = 0$) and then the case with a finite gate voltage $U \neq 0$.

A. Zero gate voltage

In Fig. 5(a) we plot G , R_A , and N , as functions of the bias voltage applied across the junction, for a GNR with even N_W , and in Fig. 5(b) we plot the same quantities for a GNR with odd N_W . In the subgap regime $eV < \Delta_0$ a striking dependence on the number of sites arises. While for even N_W the AR coefficient R_A vanishes, the opposite occurs for odd N_W , where R_A is unity. Because for $eV < \Delta_0$ electron transport is possible only by virtue of AR processes, the conductance G also vanishes in this voltage range for even N_W . In contrast, for odd N_W , G

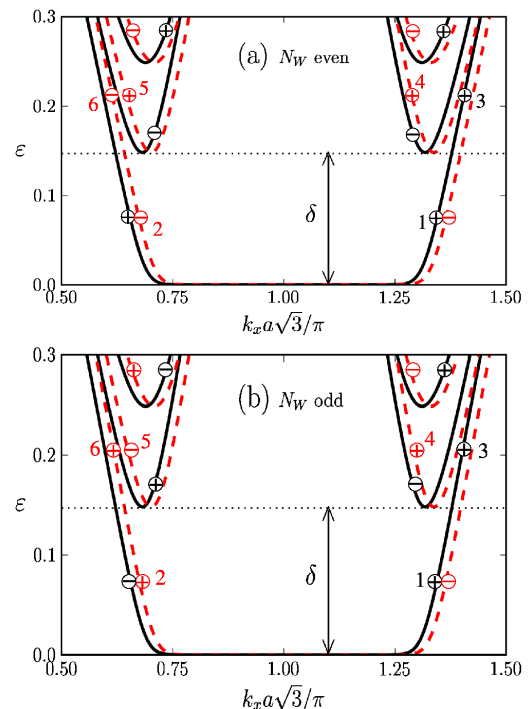


FIG. 3: (Color online) The band structure of a GNR as a function of the longitudinal wavevector k_x . Only the three lowest bands are illustrated. Energies are in units of γ . The solid (dashed) lines represent the particle (hole) bands. In this figure $U = 0$ (zero gate voltage). In this case particle and hole bands are degenerate (for the sake of clarity the hole bands have been slightly shifted to the right). The signs + and - inside the circles indicate the value η of pseudoparity for each band. (a) N_W is even. In the range $0 < \varepsilon < \delta$ no AR is possible, since left-moving hole states “2” have pseudoparity opposite to the one of incoming right-moving particle states “1”. In contrast, for $\varepsilon > \delta$, left-moving hole states “4” and “5” with the same pseudoparity as incoming particle states “3” are available, and AR is finite. (b) N_W is odd. In this case AR is possible in the range $0 < \varepsilon < \delta$ since left-moving hole states “2” have the same pseudoparity of incoming right-moving particle states “1”. For $\varepsilon > \delta$ left-moving hole states “4” and “6” with the same pseudoparity as incoming particle states “3” are available and AR is again possible. Note that left-moving hole state “5” in this case has pseudoparity opposite to the one of incoming right-moving particle states “3”.

takes its maximum value in the same voltage range. In the regime $\Delta_0 < eV < \delta$, where quasi-particle transmission becomes possible, R_A drops abruptly to zero also for odd N_W . This is due to the fact that the transmission processes, which are characterized by a small momentum transfer (intra-valley), largely dominate over AR processes, which instead involve large momentum transfer (inter-valley). We thus find a finite conductance with a value equal to the number N of open channels (in units of $4e^2/h$). Finally, for $eV > \delta$, R_A is finite but quite small in both cases (for clarity R_A has been multiplied

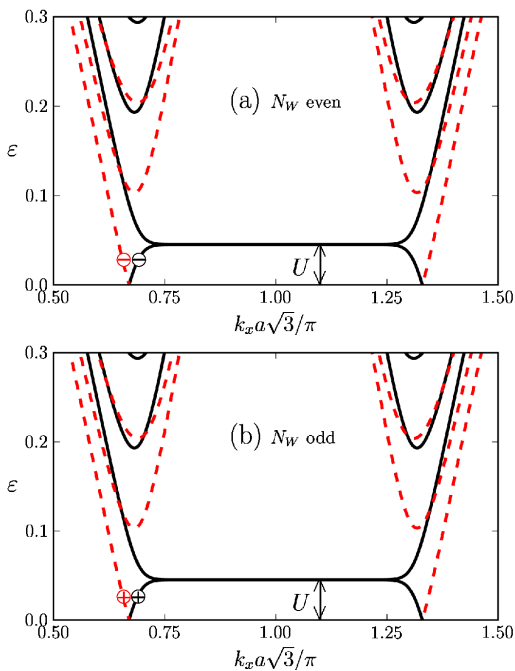


FIG. 4: (Color online) Same as in Fig. 2 but for $U \neq 0$ (finite gate voltage). In this case for $\varepsilon < U$ incoming particle states and outgoing hole states have the same pseudoparity, and AR is allowed.

by an enhancement factor), since voltages in this range are well above the superconducting gap.

These features ($R_A = 0$ for $eV < \delta$ if N_W is even and $R_A = 1$ for $eV < \Delta_0$ if N_W is odd) can be understood in terms of a pseudoparity superselection rule for the scattering states of the GNR. Let us consider a right-moving incoming electron (labeled by “1” in Fig. 2) with an energy lying between ε_F and the bottom of the second band. The only hole state available for an AR process is the one labeled by “2”, which is characterized by a pseudoparity η that is (i) *opposite* to the one of the incoming electron for even N_W and (ii) *equal* to the one of the incoming electron for odd N_W .

A superconducting parameter that is constant along the transverse direction cannot couple states with opposite pseudoparity (*i.e.* the pseudoparity of an electron impinging onto the SC interface cannot be flipped). Thus for even N_W the AR process is forbidden and R_A vanishes, whereas for odd N_W this process is allowed and R_A is finite. Notice that in the latter case normal reflection is forbidden by pseudoparity conservation, yielding $R_A = 1$ in the subgap regime. For $\Delta_0 < eV < \delta$ normal transmission is the dominating process, so that R_A is strongly suppressed for both even and odd N_W . A finite AR is restored for $eV > \delta$. Indeed in this case intra-valley scattering into hole states with the appropriate pseudoparity [“4” in Figs. 3(a) and Fig. 3(b)] is available. This superselection rule is the ribbon counterpart of the bulk Klein-paradox selection rules based on pseudospin² and

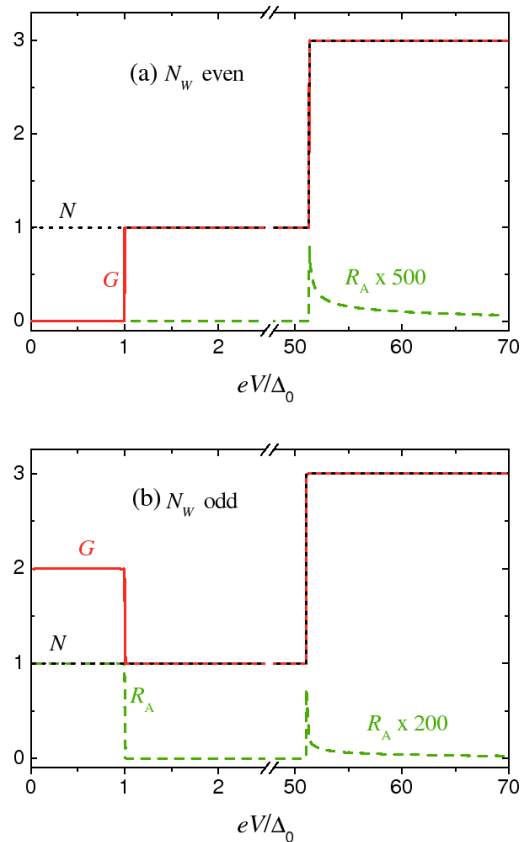


FIG. 5: (Color online) Transport properties of a GNR/SC interface. The differential conductance G in units of $4e^2/h$ (solid line), the total Andreev-reflection coefficient R_A (dashed line), and the number N of open channels (dotted line) are shown as functions of the applied bias eV (in units of Δ_0). Note that the horizontal axis has been broken in two ranges. The GNR has a width of about 50 nm, which corresponds to $\delta \sim 52 \text{ meV} = 52 \Delta_0$ (the superconducting gap has been fixed at the value $\Delta_0 = 1 \text{ meV}$). (a) $N_W = 250$. The AR coefficient is non-zero only for $eV > \delta$, and has been multiplied by a factor 500 for clarity. (b) $N_W = 251$. The AR coefficient is unity for $eV < \Delta_0$ and drops abruptly to zero for $eV > \Delta_0$, remaining zero up to $eV = \delta$. The AR coefficient is again finite for $eV > \delta$, and has been multiplied by a factor 200 for clarity.

also explains the valley-valve effect in p-n junctions in GNRs^{20,21,22}.

B. Finite gate voltage

Let us now consider the case $U \neq 0$ (and $U \ll \delta$). In Fig. 6 we plot our results for G , R_A , and N .

A comparison between Fig. 5(a) and Fig. 6(a) shows that the application of a gate voltage has dramatic consequences on electron conduction in GNRs with even N_W . This is evident from Fig. 4(a). AR processes are allowed by pseudoparity conservation in the bias range

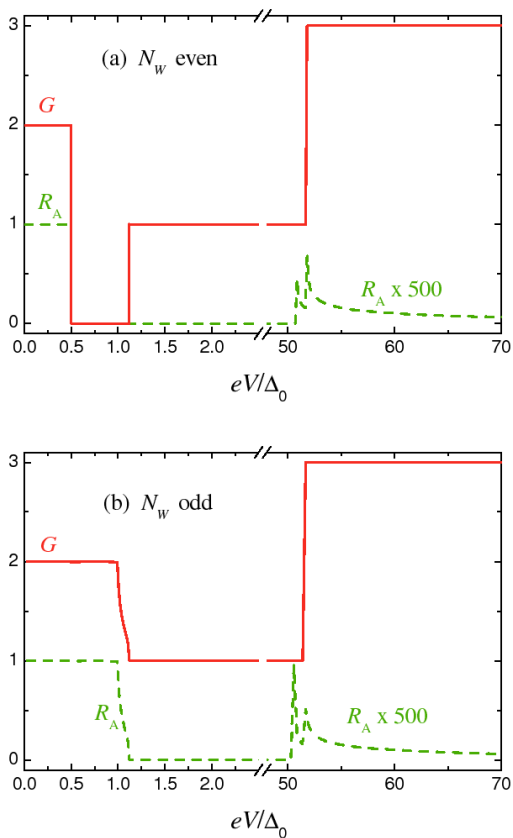


FIG. 6: (Color online) Same as in Fig. 5 but for $U = 0.5 \Delta_0$ (in this figure we have not plotted the number of open channels). (a) N_W even. In this case the AR coefficient is restored to a finite value for $eV < U$, while it remains zero for $U < eV < \delta$. (b) N_W odd. In this case no big qualitative changes are seen to occur by switching on a finite value of U .

$eV < U$, while they are forbidden for $U < eV < \delta$. This fact is reflected in the results shown in Fig. 6(a), where the differential conductance is finite (and equal to $8e^2/h$) for $eV < U$ and vanishes in the range²⁹ $U < eV < \sqrt{U^2 + \Delta_0^2}$. For subgap voltages electron conduction can be switched on and off by the application of a gate voltage. The junction between an even- N_W GNR and a SC exhibits the operational behavior of an electron transistor based on the pseudoparity conservation law.

In contrast, for odd N_W the application of a gate voltage is expected to have no major qualitative impact on the transport properties of a junction between a GNR with odd N_W and a SC. Once again, this expectation can be traced back to the pseudoparity quantum number, as depicted in Fig. 4(b). The data reported in Fig. 6(b) show indeed the same qualitative behavior reported in Fig. 5(b). The only slight modification is that the drop of R_A to zero, in the range $eV \gtrsim \Delta_0$, is less abrupt than

in Fig. 5(b), due to a slight momentum mismatch in the transmission channel between GNR and S sides, arising when $U \neq 0$.

Before concluding we would like to comment on the double-spike structure of R_A at voltages $eV = \delta \pm U$, which is seen in both panels of Fig. 6. This is due to the opening of new channels for AR processes made available by the existence of the first-excited energy band (see Fig. 4).

IV. CONCLUSIONS

In summary, we have studied Andreev reflection in graphene nanoribbon/superconductor hybrid junctions.

We have reported analytical expressions for the eigenfunctions of the tight-binding Hamiltonian describing the graphene nanoribbon, which are valid at arbitrary energy and carry explicitly a definite pseudoparity. The superselection rule stemming from this quantum number has two main implications on transport through the hybrid junction. For narrow nanoribbons with an even number of sites in the transverse direction we have found a complete suppression of Andreev reflection in a range of energies that is huge when the Fermi energy lies at the Dirac level. This implies zero conductance at subgap voltages, which can however be restored applying a finite gate potential, opening up potential technological applications of these hybrid junctions as electron transistors as well as nanorefrigerators. In contrast, in the case of narrow nanoribbons with an odd number of sites we have found perfect Andreev reflection at subgap voltages and an abrupt suppression of it at supergap voltages.

The study of non-ideal edges, realistic interfaces, and bulk disorder is beyond the scope of the present work and is postponed to a future publication³⁰. The role of electron-electron interactions and/or next nearest-neighbor hopping, which also has not been addressed in the present work, can be qualitatively understood along the following lines. These effects have been shown to lead to the opening of a gap Δ_g at the Dirac level^{1,16}, which is however typically much smaller than δ . Our conclusions thus remain valid for a large range of energies even when these effects are taken into account.

Acknowledgments

We gratefully acknowledge Carlo Beenakker and Francisco Guinea for very useful discussions and suggestions. This work has been partly supported by the NANOFRIDGE EU Project and by the CNR-INFM ‘‘Seed Projects’’.

- ¹ A.K. Geim and K.S. Novoselov, *Nature Mater.* **6**, 183 (2007); A.K. Geim and A.H. MacDonald, *Phys. Today* **60**(8), 35 (2007); A.H. Castro Neto, F. Guinea, N.M.R. Peres, K.S. Novoselov, and A. K. Geim, arXiv:0709.1163v2.
- ² M.I. Katsnelson, K.S. Novoselov, and A.K. Geim, *Nature Phys.* **2**, 620 (2006).
- ³ C.W.J. Beenakker, *Phys. Rev. Lett.* **97**, 067007 (2006); M. Titov and C.W.J. Beenakker, *Phys. Rev. B* **74**, 041401(R) (2006); C.W.J. Beenakker, arXiv:0710.3848v2.
- ⁴ T. Ludwig, *Phys. Rev. B* **75**, 195322 (2007).
- ⁵ J. Linder and A. Sudbø, *Phys. Rev. Lett.* **99**, 147001 (2007) and *Phys. Rev. B* **77**, 064507 (2008).
- ⁶ J.C. Cuevas and A. Levy Yeyati, *Phys. Rev. B* **74**, 180501 (2006).
- ⁷ J. Cayssol, *Phys. Rev. Lett.* **100**, 147001 (2008).
- ⁸ E. Prada, P. San-Jose, B. Wunsch, and F. Guinea, *Phys. Rev. B* **75**, 113407 (2007).
- ⁹ See for example S. Bhattacharjee and K. Sengupta, *Phys. Rev. Lett.* **97**, 217001 (2006); A.G. Moghaddam and M. Zareyan, *Phys. Rev. B* **74**, 241403(R) (2006); M. Titov, A. Ossipov, and C.W.J. Beenakker, *ibid.* **75**, 045417 (2007); A.R. Akhmerov and C.W.J. Beenakker, *ibid.* **75**, 045426 (2007); A. Ossipov, M. Titov, and C.W. J. Beenakker, *ibid.* **75**, 241401(R) (2007); D. Greenbaum, S. Das, G. Schwiete, and P. G. Silvestrov, *ibid.* **75**, 195437 (2007); M. Maiti and K. Sengupta, *ibid.* **76**, 054513 (2007); J. Gonzalez and E. Perfetto, *ibid.* **76**, 155404 (2007); S. Bhattacharjee, M. Maiti, and K. Sengupta, *ibid.* **76**, 184514 (2007); G. Tkachov, *ibid.* **76**, 235409 (2007); K. Sasaki *et al.*, *J. Phys. Soc. Jpn.* **76**, 033702 (2007); B. Uchoa and A.H. Castro Neto, *Phys. Rev. Lett.* **98**, 146801 (2007); A.R. Akhmerov and C.W.J. Beenakker, *ibid.* **98**, 157003 (2007); C.W.J. Beenakker, A.R. Akhmerov, P. Recher, and J. Tworzydło, *Phys. Rev. B* **77**, 075409 (2008); T. Yokoyama, J. Linder, and A. Sudbo, *ibid.* **77**, 132503 (2008); P. Buset, A. Levy Yeyati, and A. Martín-Rodero, *ibid.* **77**, 205425 (2008); J. Linder, T. Yokoyama, D. Huertas-Hernando, and A. Sudbø, *Phys. Rev. Lett.* **100**, 187004 (2008); C. Benjamin and J.K. Pachos, arXiv:0802.3181v1; A.M. Black-Schaffer and S. Doniach, arXiv:0803.3574v1; M. Zareyan, H. Mohammadpour, and A.G. Moghaddam, arXiv:0804.2774v1 and other related works cited in these papers.
- ¹⁰ A.F. Andreev, *Sov. Phys. JETP* **19**, 1228 (1964).
- ¹¹ A. Shailos, W. Nativel, A. Kasumov, C. Collet, M. Ferrer, S. Gueron, R. Deblock, and H. Bouchiat, arXiv:cond-mat/0612058v2.
- ¹² F. Miao, S. Wijeratne, U. Coskun, Y. Zhang, and C.N. Lau, arXiv:cond-mat/0703052v2.
- ¹³ H.B. Heersche, P. Jarillo-Herrero, J.B. Oostinga, L.M.K. Vandersypen, and A.F. Morpurgo, *Nature* **446**, 56 (2007).
- ¹⁴ X. Du, I. Skachko, and E.Y. Andrei, *Phys. Rev. B* **77**, 184507 (2008).
- ¹⁵ Z. Chen, Y.-M. Lin, M.J. Rooks, and P. Avouris, *Physica E* **40**, 228 (2007); M.Y. Han, B. Özyilmaz, Y. Zhang, and P. Kim, *Phys. Rev. Lett.* **98**, 206805 (2007); X. Li, X. Wang, L. Zhang, S. Lee, and H. Dai, *Science* **319**, 1229 (2008); X. Wang, Y. Ouyang, X. Li, H. Wang, J. Guo, and H. Dai, *Phys. Rev. Lett.* **100**, 206803 (2008); Y.-M. Lin, V. Perebeinos, Z. Chen, and P. Avouris, arXiv:0805.0035v2.
- ¹⁶ See *e.g.* Y.-W. Son, M.L. Cohen, and S.G. Louie, *Phys. Rev. Lett.* **97**, 216803 (2006); V. Barone, O. Hod, and G.E. Scuseria, *Nano Lett.* **6**, 2748 (2006); L. Yang, C.-H. Park, Y.-W. Son, M.L. Cohen, and S.G. Louie, *Phys. Rev. Lett.* **99**, 186801 (2007).
- ¹⁷ L. Brey and H.A. Fertig, *Phys. Rev. B* **75**, 125434 (2007).
- ¹⁸ L. Malysheva and A. Onipko, *Phys. Rev. Lett.* **100**, 186806 (2008).
- ¹⁹ A.R. Akhmerov and C.W. Beenakker, *Phys. Rev. B* **77**, 085423 (2008).
- ²⁰ K. Wakabayashi and T. Aoki, *Int. J. Mod. Phys. B* **16**, 4897 (2002).
- ²¹ A.R. Akhmerov, J.H. Bardarson, A. Rycerz, and C.W.J. Beenakker, *Phys. Rev. B* **77**, 205416 (2008).
- ²² A. Cresti, G. Grosso, and G. Pastori Parravicini, *Phys. Rev. B* **77**, 233402 (2008).
- ²³ For any $k_x \in [0, 2\pi/(a\sqrt{3})[$ the equation has N_W real solutions $k_y \in]0, 2\pi/(3a)[$, except in the range $2\pi/3 \lesssim k_x a\sqrt{3} \lesssim 4\pi/3$ where one solution is imaginary and corresponds to the evanescent wave of the zero mode, see M.I. Katsnelson and F. Guinea, arXiv:0804.2348v1; A. Rycerz and C.W.J. Beenakker, arXiv:0709.3397v1; A. Rycerz, arXiv:0710.2859v2.
- ²⁴ A. Rycerz, J. Tworzydło, and C.W.J. Beenakker, *Nature Phys.* **547**, 172 (2007).
- ²⁵ P.G. de Gennes, *Superconductivity of Metals and Alloys* (Addison-Wesley, New York, 1989).
- ²⁶ Notice that, since graphene honeycomb lattice is bipartite, a simplified model in which Δ_i is assumed as a step-like function along the \hat{e}_x direction would effectively imply a rapid variation of Δ_i also transversally along the two-site cells. Since such situation would not be realistic, we have adopted a smooth variation of Δ_i , over a length $\lambda \simeq 10a$ along the \hat{e}_x direction.
- ²⁷ S. Datta, *Electronic Transport in Mesoscopic Systems*, (Cambridge Studies in Semiconductor Physics and Micro-electronic Engineering, Cambridge, 1995).
- ²⁸ G.E. Blonder, M. Tinkham, and T.M. Klapwijk, *Phys. Rev. B* **25**, 4515 (1982); C.J. Lambert, *J. Phys. C* **3**, 6579 (1991); C.J. Lambert and R. Raimondi, *ibid.* **10**, 901 (1998).
- ²⁹ The fact that G vanishes in the range $\Delta_0 < eV < \sqrt{U^2 + \Delta_0^2}$ can also be understood in terms of pseudoparity conservation.
- ³⁰ D. Rainis *et al.*, in preparation.